



This is the accepted manuscript made available via CHORUS. The article has been published as:

## Accelerated Adiabatic Passage of a Single Electron Spin Qubit in Quantum Dots

Xiao-Fei Liu, Yuta Matsumoto, Takafumi Fujita, Arne Ludwig, Andreas D. Wieck, and Akira Oiwa

Phys. Rev. Lett. **132**, 027002 — Published 12 January 2024

DOI: [10.1103/PhysRevLett.132.027002](https://doi.org/10.1103/PhysRevLett.132.027002)

# Accelerated adiabatic passage of a single electron spin qubit in quantum dots

Xiao-Fei Liu<sup>1,2,\*</sup>, Yuta Matsumoto<sup>1</sup>, Takafumi Fujita<sup>1</sup>, Arne Ludwig<sup>3</sup>, Andreas D. Wieck<sup>3</sup> and Akira Oiwa<sup>1,4,5,6,†</sup>

<sup>1</sup>*SANKEN, Osaka University, 8-1 Mihogaoka, Ibaraki, Osaka 567-0047, Japan*

<sup>2</sup>*Beijing Academy of Quantum Information Sciences, Beijing 100193, China*

<sup>3</sup>*Lehrstuhl für Angewandte Festkörperphysik, Ruhr-Universität Bochum, Universitätsstraße 150, Gebäude NB, D-44780 Bochum, Germany*

<sup>4</sup>*Center for Quantum Information and Quantum Biology (QIQB), Osaka University, Osaka 565-0871, Japan*

<sup>5</sup>*Center for Spintronics Research Network (CSRN),*

*Graduate School of Engineering Science, Osaka University, Osaka 560-8531, Japan*

<sup>6</sup>*Spintronics Research Network Division, OTRI, Osaka University, Osaka 565-0871, Japan*

(Dated: December 11, 2023)

Adiabatic processes can keep the quantum system in its instantaneous eigenstate, which is robust to noises and dissipation. However, it is limited by sufficiently slow evolution. Here, we experimentally demonstrate the transitionless quantum driving (TLQD) of the shortcuts to adiabaticity (STA) in gate-defined semiconductor quantum dots (QDs) to greatly accelerate the conventional adiabatic passage for the first time. For a given efficiency of quantum state transfer, the acceleration can be more than 2-fold. The dynamic properties also prove that the TLQD can guarantee fast and high-fidelity quantum state transfer. In order to compensate for the diabatic errors caused by dephasing noises, the modified TLQD is proposed and demonstrated in experiment by enlarging the width of the counter-diabatic drivings. The benchmarking shows that the state transfer fidelity of 97.8% can be achieved. This work will greatly promote researches and applications about quantum simulations and adiabatic quantum computation based on the gate-defined QDs.

*Introduction.*— Gate-defined semiconductor quantum dots (QDs) can electrically control electron and hole states with ultra-high precision, which is one of the state-of-the-art quantum devices [1, 2]. The spin qubit of QDs is a promising candidate for fault-tolerant solid-state quantum computing due to its high-fidelity quantum operation [3–6], potential scalability [7–9], and well compatibility with manufacturing technology of semiconductor industry [10]. Recently, two-qubit gate fidelity of more than 99% have been demonstrated experimentally [11–14], crossing the well-known surface code threshold [15, 16]. Besides, QD systems are becoming emerging platforms for quantum simulations to explore strongly interacting electrons and topological phases in condensed-matter physics, such as the Fermi–Hubbard system [17], Nagaoka ferromagnetism [18], and the Su–Schrieffer–Heeger model [19].

In order to achieve the so called “quantum advantage” [20], a high-fidelity quantum processor with large enough computational space and programmable qubits is required. Meanwhile, it also needs accurate quantum control and good robustness against noises and dissipation. One possible pathway is to find a feasible quantum control theory that is applicable for the large-scale quantum processor and guarantees high-accuracy quantum operation simultaneously. It is well known that the manipulation of a quantum state using resonant pulses is sensitive to timing and pulse area errors. In contrast, adiabatic passage can always keep some properties of a dynamical

quantum system invariant, ideally switch an initial state into the target state, such as the high fidelity adiabatic process demonstrated in <sup>31</sup>P electron qubit of silicon QDs system [21]. This can well prevent decoherence from experimental imperfections [22]. Generally, slow enough evolution is necessary to satisfy adiabatic conditions, limiting its applications. To achieve rapid and robust quantum state manipulation, several shortcuts to adiabaticity (STA) schemes are put forward to compensate for the nonadiabatic errors [23–27], for instance the transitionless quantum driving (TLQD) and invariant-based inverse engineering. Some of them have been demonstrated in other quantum systems [28–33]. Besides, STA has significant applications in quantum simulations to greatly suppress diabatic excitations [34].

Here, we experimentally demonstrate the STA of a single spin qubit in gate-defined QDs for the first time. The experiment is based on the theory of TLQD [23], and the acceleration of quantum state transfer has been achieved. This is also verified from the dynamics of the spin state. To suppress the noises from nuclear spin fluctuations, we propose and experimentally demonstrate a modified TLQD (MOD-TLQD) by enlarging the width of the counter-diabatic pulse. The benchmarking of this MOD-TLQD demonstrates a state transfer efficiency of 97.8%. Since the gate-defined QDs are moving toward the scalable quantum processor [35], the results of this paper will greatly promote related researches about quantum control and quantum simulations.

*The acceleration of quantum state transfer.*— Figure 1(a) shows a scanning electron microscope (SEM) picture of the double QDs (DQDs), which is fabricated on the GaAs/AlGaAs heterostructure. After the implemen-

\* liuxf@baqis.ac.cn

† oiwa@sanken.osaka-u.ac.jp

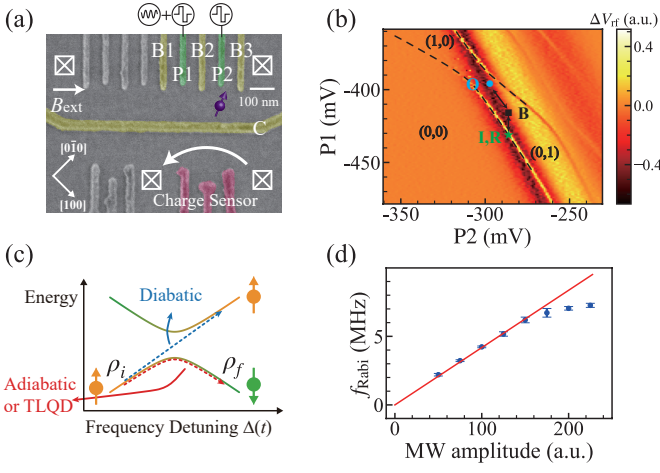


Figure 1. The device and its basic properties. (a) The false-colored micrograph of the device. The high frequency pulses are applied through the plunger gates P1 and P2, and the MW driving is connected with P1. (b) Charge stability diagram around single electron region. The position of I, B, and O are represented by the green star, black square, and blue circle, respectively. The position of the initialization is also used for the readout. (c) The schematic of TLQD. (d) Rabi frequency  $f_{\text{Rabi}}$  as a function of the MW amplitude. Its maximum value is about  $f_{\text{Rabi}}^{\text{max}} \sim 7.5$  MHz.

tation of an in-plane magnetic field  $B_{\text{ext}}$ , the qubit frequency of a single electron spin is  $f_{\text{qubit}} = |g|\mu_B B / (2\pi\hbar)$ , in which  $\mu_B$  is the Bohr magneton,  $g$  is the Landé  $g$ -factor ( $\sim -0.41$  for this GaAs QDs), and  $B$  is the total magnetic field (consists of  $B_{\text{ext}}$  and the effective Overhauser field  $B_{\text{nuc}}^z$ ). When a microwave (MW) driving is applied, the spin manipulation can be achieved using electric dipole spin resonance (EDSR) [36]. Besides, we use inter-dot tunneling to enhance the Rabi frequency [37]. We employ energy-selective readout to measure the spin state [38–40]. A nearby charge sensor provides rapid and real time detection of charge state based on the radio frequency (RF) reflectometry [41, 42].

Under the rotating frame, the interaction Hamiltonian expanded on the  $|\uparrow\rangle$  and  $|\downarrow\rangle$  Hilbert space is

$$\hat{H}_0 = \frac{\hbar}{2} \begin{pmatrix} -\Delta(t) & \Omega_R(t) \\ \Omega_R(t) & \Delta(t) \end{pmatrix}, \quad (1)$$

in which  $\Omega_R(t)$  is the Rabi frequency, and  $\Delta(t)$  is the frequency detuning with the expression  $\Delta(t) = \omega_{\text{qubit}} - \omega_{\text{MW}} - t\dot{\omega}_{\text{MW}}$ . A high-fidelity quantum state transfer can occur if the evolution of this controllable parameter  $\Delta(t)$  is slow enough. However, the TLQD can correct diabatic errors by adding the counter-diabatic driving  $\hat{H}_{\text{CD}}$  even though the evolution does not satisfy adiabatic conditions [23], as shown in Fig. 1(c). The TLQD can always keep the system in  $|\varphi_k(t)\rangle$ , the instantaneous eigenstate of  $\hat{H}_0$ . Therefore, the time-dependent evolution operator and total Hamiltonian can be obtained. Furthermore, we can know  $\hat{H}_{\text{CD}}$  which has the expression  $i\hbar \sum_k |\partial_t \varphi_k\rangle \langle \varphi_k|$ . For this single electron spin

system, its specific expression is  $\hat{H}_{\text{CD}} = \hbar\Omega_a(t) \sigma_y / 2$ , in which  $\Omega_a(t) = [\Omega_R(t) \dot{\Delta}(t) - \dot{\Omega}_R(t) \Delta(t)] / \Omega^2$  and  $\Omega^2 = \Delta^2(t) + \Omega_R^2(t)$ . Obviously, the function of  $\hat{H}_{\text{CD}}$  is to correct the diabatic errors by applying a time-dependent driving in  $\hat{y}$ -axis.

In our experiment, the electron is initialized to  $|\uparrow\rangle$  state at the initialization point (I), as shown in Fig. 1(b). Then, the pulse sequences applied on plunger gates P1 and P2 deliver this electron to the intermediate transit point (B) and then to the operation point (O). After the spin manipulation at O point, this electron is delivered back to B and then to the readout point (R). Here, I and R point are the same. Our setup utilizes an arbitrary waveform generator (AWG) and an I/Q mixer to precisely tune the time-dependent terms  $\Omega_R$ ,  $\Omega_a$ , and  $\Delta$ . The relationship between  $\Omega_R$  (or  $\Omega_a$ ) and the MW amplitude has to be characterized firstly. The Rabi frequency estimated from the Rabi oscillation and Landau-Zener transition are nearly the same. Please find more details in Section III of the Supplementary Materials. As shown in Fig. 1(d),  $f_{\text{Rabi}}$  increases linearly with larger MW amplitude. Then, it becomes saturated progressively until reaching the maximum value  $f_{\text{Rabi}}^{\text{max}} \sim 7.5$  MHz because of the limitation from the trapping potentials or MW amplifiers.

The most significant advantage of this TLQD is that it can always guarantee a quantum system in one of its instantaneous eigenstates and greatly accelerate the adiabatic passage. Figure 2(a) shows the final spin down probability  $P_{\downarrow}$  and state transfer efficiency (or fidelity)  $F_{\text{flip}}$  as a function of the total evolution time  $T_e$ . The green squares and blue circles represent the results of TLQD and conventional adiabatic evolution, respectively. The red solid line is the least-squares fitting to the Landau-Zener formula [43–45]. The experimental results show that TLQD always has higher  $P_{\downarrow}$  and  $F_{\text{flip}}$  than the conventional adiabatic passage. The differences of  $P_{\downarrow}$  (also  $F_{\text{flip}}$ ) between TLQD and adiabatic passage become smaller progressively with longer  $T_e$  (slower evolution speed). When  $T_e$  is long enough,  $\Omega_a$  becomes small enough to be neglected, in analogy to the adiabatic evolution. Note that  $F_{\text{flip}}$  is evaluated from the experimental results  $P_{\downarrow}$  by taking the initialization fidelity ( $F_{\text{ini}}^{\uparrow}$ ), spin-to-charge fidelity ( $F_{\text{STC}}^{\downarrow}$  and  $F_{\text{STC}}^{\uparrow}$ ), and charge detection fidelity ( $F_E$ ) into consideration. Please check Section I and VI in the Supplementary Materials. Generally, the relationship  $P_{\downarrow} = P_{\downarrow}^{\text{ini}=\uparrow} + P_{\downarrow}^{\text{ini}=\downarrow}$  exists, in which  $P_{\downarrow}^{\text{ini}=\uparrow}$  and  $P_{\downarrow}^{\text{ini}=\downarrow}$  stand for the situations with the initialization of spin to up and down state, respectively. The expression of  $P_{\downarrow}^{\text{ini}=\uparrow}$  and  $P_{\downarrow}^{\text{ini}=\downarrow}$  are  $F_{\text{ini}}^{\uparrow} F_{\text{flip}} F_{\text{STC}}^{\downarrow} F_E + F_{\text{ini}}^{\uparrow} (1 - F_{\text{flip}}) (1 - F_{\text{STC}}^{\downarrow}) F_E$  and  $(1 - F_{\text{ini}}^{\uparrow}) (1 - F_{\text{flip}}) F_{\text{STC}}^{\downarrow} F_E + (1 - F_{\text{ini}}^{\uparrow}) F_{\text{flip}} (1 - F_{\text{STC}}^{\downarrow}) F_E$ , respectively. We also make sure that the enhancement of state transfer originates from the compensation for diabatic errors instead of simply enlarging the Rabi frequency, please see Section II in the Supplementary Ma-

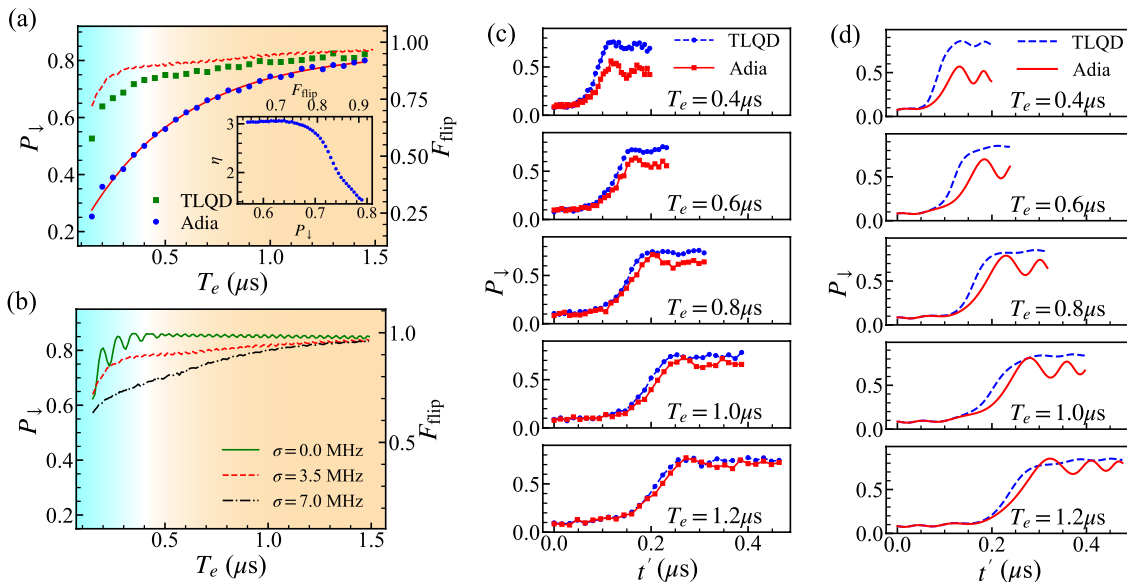


Figure 2. The result of TLQD. (a) The final spin down probability  $P_{\downarrow}$  as a function of the evolution time  $T_e$  using the conventional adiabatic evolution and TLQD. The red solid line is the fitting to the formula  $AP_{\downarrow}^{LZ} + B$ , giving the value of  $\Omega_R/2\pi = 4.63$  MHz. The inset displays the speed-up factor  $\eta$  as functions of  $P_{\downarrow}$  and the efficiency of state transfer  $F_{\text{flip}}$ . (b) The simulation results of  $P_{\downarrow}$  and  $F_{\text{flip}}$  as a function of  $T_e$  under different variance of qubit frequency noise  $\sigma \sim 0.0$  MHz (green solid line), 3.5 MHz (red dashed line), and 7.0 MHz (black dashdotted line). To better compare the simulation and experimental results, the red dashed line with  $\sigma \sim 3.5$  MHz is also plotted in (a). The modulation depth is  $\delta_d = 100.0$  MHz. The maximum Rabi frequency is assumed to be  $f_{\text{Rabi}}^{\text{max}} = 7.5$  MHz. (c) and (d) are the experimental and simulation results of the dynamics of  $P_{\downarrow}$ , respectively. The Rabi frequency is  $\Omega_R/2\pi = 4.18$  MHz.

terials. In our experiment, the maximum value of  $P_{\downarrow}$  is about 0.85, which is mainly limited by the readout fidelity. It can be improved by enhancing the relaxation time  $T_1$  and bandwidth of the RF-reflectometry after demodulation.

We find that  $P_{\downarrow}$  and  $F_{\text{flip}}$  of TLQD decrease more rapidly when  $T_e < 0.4 \mu\text{s}$ . This originates from the saturation of  $\Omega_a$  (because of the large compensation for diabatic errors and the limited value of  $f_{\text{Rabi}}^{\text{max}}$ ). Please find the simulation results without considering the limitation of  $f_{\text{Rabi}}^{\text{max}}$  in Fig. S13 of the Supplementary Materials. When  $T_e > 0.4 \mu\text{s}$ , there is a tiny increase of  $P_{\downarrow}$  and  $F_{\text{flip}}$ . As you can see in Section II of the Supplementary Materials, the TLQD has the highest efficiency of state transfer when  $f_{\text{qubit}} = f_{\text{MW}}^c$  ( $f_{\text{MW}}^c$  is the center frequency of the MW). The dephasing noises (mainly from the Overhauser field) would cause the fluctuations of  $B_{\text{nuc}}^z$  and degrade the performance of TLQD.

The simulation after taking dephasing noises and saturation of Rabi frequency into consideration is also performed. For the GaAs QDs [46, 47], the coherence time is dominated by the quasistatic (or low-frequency) noises with a spectral distribution  $S(f) \propto 1/f^\beta$ . For simplicity,  $\beta$  is set to be 2, i.e.,  $S(f) = A^2/f^2$ . The variance of the qubit frequency  $\sigma$  can be estimated as  $\sigma^2 = 2 \int_{f_c}^{1/t} S(f) df = 2A^2(1/f_c - t)$ . Here,  $f_c$  and  $1/t$  are low and high cutoff frequencies, respectively. The value of  $A$  can be calculated from the Ramsey pat-

tern. Using the relationship  $1/T_2^* = \sqrt{2\pi}\sigma$ , we know  $1/T_2^* = 2\pi A \sqrt{1/f_c - t}$ . Please find more details in Section V of the Supplementary Materials. Here, the saturation value of total Rabi frequency is  $f_{\text{Rabi}}^{\text{max}} = 7.5$  MHz, i.e.,  $\Omega(t)$  is set as 7.5 MHz if  $\Omega(t) > f_{\text{Rabi}}^{\text{max}}$ . The value of  $\sigma$  is about 3.5 MHz. The simulation result is plotted as the red dashed line in both Fig. 2(a) and (b), which can well reproduce experimental results qualitatively. For GaAs QDs,  $\beta$  may range between 1 and 3. This just changes the value of  $A$  without changing the estimation of  $\sigma$  too much. In our simulation, we generate 2000 random values of  $\delta f_{\text{qubit}}$  (the shift of the qubit frequency) with the variance  $\sigma$ . For each  $\delta f_{\text{qubit}}$ , we can know  $F_{\text{flip}}$  (also  $P_{\downarrow}$  based on the relationship with  $F_{\text{flip}}$ ) by solving the Schrödinger equation of  $\hat{H}_0 + \hat{H}_{\text{CD}}$ . The average values of  $F_{\text{flip}}$  and  $P_{\downarrow}$  are the simulation results.

Generally, the TLQD consumes less time compared with conventional adiabatic evolution for a given state transfer efficiency. This acceleration can be characterized quantitatively by the time ratio  $\eta = T_{\text{adia}}/T_{\text{TLQD}}$ , in which  $T_{\text{TLQD}}$  and  $T_{\text{adia}}$  represent the time using the TLQD and conventional adiabatic passage, respectively. The result is shown in the inset of Fig. 2(a), in which an acceleration of more than 2-fold can be achieved. The value of  $\eta$  becomes flat when  $P_{\downarrow} < 0.65$ , which is due to the limitation of  $f_{\text{Rabi}}^{\text{max}}$ . Note that  $T_{\text{TLQD}}$  is estimated from the polynomial fitting to the experimental results of TLQD, and  $T_{\text{adia}}$  is deduced from the fitting to the

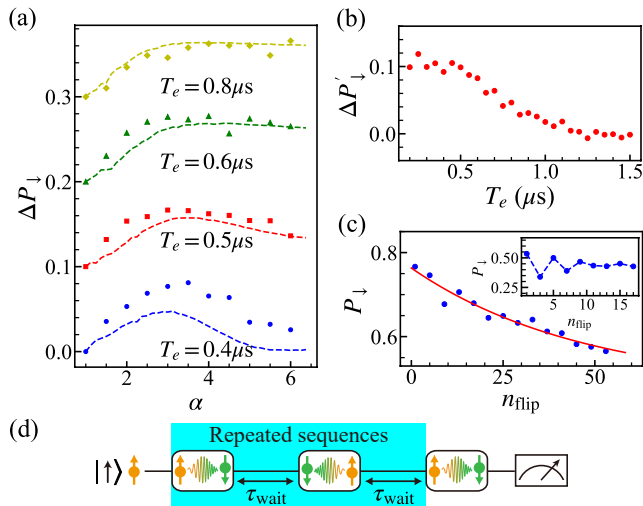


Figure 3. The result of MOD-TLQD. (a) The enhancement of spin flip probability  $\Delta P_{\perp}$  as a function of  $\alpha$  under different  $T_e$ . The markers are experimental data, and the lines represent simulation results. The variance of qubit frequency is  $\sigma \sim 2.9$  MHz. The traces are shifted vertically for clarity. (b) The enhancement of spin flip probability  $\Delta P'_{\perp}$  as a function of  $T_e$ . The width factor is set to be  $\alpha = 2.5$ . The Rabi frequency in (a) and (b) is  $\Omega_R/2\pi \sim 4.0$  MHz. (c) The benchmarking of the efficiency of state transfer using the MOD-TLQD, giving the value of  $p = 0.978 \pm 0.01$ . The inset corresponds to the result of conventional adiabatic evolution, which has the oscillation instead of an exponential decay. (d) The schematic of pulse sequences to benchmark the spin flip fidelity.

Landau-Zener formula. We believe that the acceleration would be much faster for QDs with longer coherence time, e.g., silicon QDs [48]. The green solid line in Fig. 2(b) shows the simulation results if  $\sigma = 0.0$  MHz. When the evolution time  $T_e > 0.4 \mu\text{s}$ ,  $P_{\perp}$  and  $F_{\text{flip}}$  can always keep the highest value. Furthermore, an acceleration of  $\eta > 6$  can be achieved from our rough estimation. In contrast, large noises would greatly lower the efficiency of state transfer, represented by the black dashdotted line.

The dynamic properties of TLQD and adiabatic evolution are also investigated experimentally, as shown in Fig. 2(c). The blue line with circle dots and red line with square dots represent the results of TLQD and conventional adiabatic evolution, respectively. Here, we just show the results starting from the time  $0.3 T_e$ , i.e., the relative time  $t'$  has a shift of  $0.3 T_e$  with respect to the real time. Simulation results are displayed in Fig. 2(d), which can well reproduce experimental results. The experimental and simulation results show that this TLQD can always keep highest  $P_{\perp}$  (also  $F_{\text{flip}}$ ) after spin flip under various  $T_e$  ranging from  $0.4 \mu\text{s}$  to  $1.2 \mu\text{s}$ . In contrast,  $P_{\perp}$  (also  $F_{\text{flip}}$ ) would increase gradually with longer  $T_e$  for the conventional adiabatic evolution. Meanwhile, its  $P_{\perp}$  has much larger amplitude of oscillation compared with TLQD after the spin flip because its quantum state is not the eigenstate of this system.

*Compensation for dephasing noises.*— For an ideal case, the efficiency of state transfer using TLQD can be up to 100%. There are two main reasons that make it difficult to realize such high efficiency. The first comes from charge noises, which may cause a shift of the O point and  $\Omega_R$ , leading to the over or under estimated value of  $\Omega_a$ . The second is the nuclear spin fluctuations which can cause the shift of qubit frequency and significant dephasing in GaAs QDs. Here, we propose a feasible and simple method through pulse optimization to greatly compensate for dephasing noises.

In the TLQD experiment demonstrated above,  $\Omega_R$  is kept as a constant and  $\Delta$  is modulated linearly. Therefore,  $\Omega_a$  has a Gaussian envelope, i.e.,  $\Omega_a(t) \propto (\Delta^2 + \Omega_R^2)^{-1}$ . In order to compensate for the dephasing noises, we can enlarge the width of this Gaussian envelope without changing the maximum value of  $\Omega_a$ . This modified pulse is  $\Omega_a^{\text{MOD}}(t) = \alpha^2 \Omega_R \Delta (\Delta^2 + \alpha^2 \Omega_R^2)^{-1}$ . Here,  $\alpha$  is the width factor, and this optimization makes the pulse width to be  $\alpha \Omega_R$ . The enhancement of  $P_{\perp}$ , with the definition  $\Delta P_{\perp}(\alpha) = P_{\perp}(\alpha) - P_{\perp}(\alpha = 1.0)$ , as a function of  $\alpha$  under various  $T_e$  is shown in Fig. 3(a). It shows that  $P_{\perp}$  would increase with  $\alpha$  firstly and reach the maximum when  $\alpha$  ranges from 2.5 to 3.0. If  $T_e < 0.6 \mu\text{s}$ , there is a clear drop of  $\Delta P_{\perp}$  when  $\alpha > 2.5$ , which may be due to the over compensation for diabatic errors. In contrast,  $\Delta P_{\perp}$  is nearly flat when  $\alpha > 2.5$  for the situation of  $T_e > 0.6 \mu\text{s}$ . The reason is that  $\Omega_a$  becomes smaller and the effect of over compensation is not obvious any more. The simulation results shown as the dashed lines can well reproduce our experimental results. We also note that the simulation result of  $T_e = 0.4 \mu\text{s}$  is much smaller than the experimental result, which may be due to the under estimated value of  $f_{\text{Rabi}}^{\text{max}}$  in our calculation.

In order to well demonstrate the performance of this width optimization method, the enhancement of  $P_{\perp}$  defined as  $\Delta P'_{\perp} = \Delta P_{\perp}(\alpha = 2.5)$  as a function of  $T_e$  is displayed in Fig. 3(b). There is a clear enhancement under various  $T_e$ . Thus, the degradation of state transfer caused by the dephasing noises can be greatly compensated using the MOD-TLQD. Meanwhile,  $\Delta P'_{\perp}$  becomes smaller progressively with longer  $T_e$  because of the negligible  $\Omega_a$ . When  $T_e > 1.1 \mu\text{s}$ ,  $\Delta P'_{\perp}$  is nearly zero. Besides, the optimal value of  $\alpha$  will become smaller with larger  $\Omega_R$  because we have to keep  $\alpha \Omega_R$  comparable with the dephasing noises. Please see more data in Section VIII of the Supplementary Materials.

Finally, the performance of this MOD-TLQD is characterized quantitatively. The probability  $P_{\perp}$  as a function of the spin flip number  $n_{\text{flip}}$  is measured, as shown in Fig. 3(c). The evolution time is  $T_e = 0.6 \mu\text{s}$ , and a waiting time  $\tau_{\text{wait}} = 0.2 \mu\text{s}$  is added after each spin flip process to reduce the thermal heating, as shown in Fig. 3(d). The repeated sequences represent two flips in a row to keep the spin up state. After fitting to the formula  $P_{\perp} = Ap^{n_{\text{flip}}} + B$ , the fidelity  $p = 0.978 \pm 0.01$  is obtained. The relationship between  $n_{\text{flip}}$  and the number of this repeated sequences  $n_{\text{seq}}$  is  $n_{\text{flip}} = 2n_{\text{seq}} + 1$ . In contrast,

the conventional adiabatic evolution has a clear oscillation for  $T_e = 0.6 \mu\text{s}$ , as shown in the inset of Fig. 3(c). Only when  $T_e$  is large enough (larger than  $1.1 \mu\text{s}$ ), the exponential decay can be observed. More data can be found in Fig. S12 of the Supplementary Materials. If we perform the spin flip using Rabi oscillation under the same conditions with Fig. 3(a), i.e.,  $\Omega_R/2\pi = 4.0 \text{ MHz}$  and  $\sigma = 2.9 \text{ MHz}$ , the spin flip fidelity is less than 65.6%. Therefore, MOD-TLQD has higher fidelity, although it takes longer time.

*Conclusion and outlook.*— The STA is experimentally demonstrated in gate-defined QDs for the first time based on the TLQD protocol. Furthermore, the optimization by enlarging the width of counter-diabatic driving can achieve the efficiency of state transfer as high as 97.8%. The acceleration of quantum state transfer would be much better in Si or Ge QDs with longer coherence time. We also find that the experimental method in our pa-

per can be directly used in the invariant-based inverse engineering [25], which also needs the precise control of time-dependent terms  $\Delta(t)$ ,  $\Omega_R(t)$ , and  $\Omega_a(t)$ . Besides, for the cases that the input is a superposition state, i.e.,  $(|\uparrow\rangle + |\downarrow\rangle)/\sqrt{2}$ , the output state would become  $(|\uparrow\rangle - |\downarrow\rangle)/\sqrt{2}$ . It means a  $\pi$  rotation along the  $\hat{z}$ -axis for this superposition state. Meanwhile, the TLQD may be used in other single-qubit operations and adiabatic passages of the QDs system. However, it still needs more researches both in theory and experiment.

This work is supported by JST CREST Grant No. JPMJCR15N2; JST Moonshot R&D Grant No. JPMJMS2066-31 and JPMJMS226B; Grant-in-Aid Scientific Research (S), 23H05458, QSP-013 from NRC, Canada; and the Dynamic Alliance for Open Innovation Bridging Human, Environment and Materials. A. L. and A. D. W. acknowledge the support of DFG-TRR160 and BMBF-QR.X Project 16KISQ009.

- 
- [1] D. Loss and D. P. DiVincenzo, Quantum computation with quantum dots, *Phys. Rev. A* **57**, 120 (1998).
- [2] R. Hanson, L. P. Kouwenhoven, J. R. Petta, S. Tarucha, and L. M. K. Vandersypen, Spins in few-electron quantum dots, *Rev. Mod. Phys.* **79**, 1217 (2007).
- [3] M. Veldhorst, J. C. C. Hwang, C. H. Yang, A. W. Leenstra, B. de Ronde, J. P. Dehollain, J. T. Muhonen, F. E. Hudson, K. M. Itoh, A. Morello, *et al.*, An addressable quantum dot qubit with fault-tolerant control-fidelity, *Nat. Nanotechnol.* **9**, 981 (2014).
- [4] M. Veldhorst, C. H. Yang, J. C. C. Hwang, W. Huang, J. P. Dehollain, J. T. Muhonen, S. Simmons, A. Laucht, F. E. Hudson, K. M. Itoh, A. Morello, and A. S. Dzurak, A two-qubit logic gate in silicon, *Nature* **526**, 410 (2015).
- [5] J. Yoneda, K. Takeda, T. Otsuka, T. Nakajima, M. R. Delbecq, G. Allison, T. Honda, T. Kodera, S. Oda, Y. Hoshi, *et al.*, A quantum-dot spin qubit with coherence limited by charge noise and fidelity higher than 99.9%, *Nat. Nanotechnol.* **13**, 102 (2018).
- [6] J. M. Nichol, L. A. Orona, S. P. Harvey, S. Fallahi, G. C. Gardner, M. J. Manfra, and A. Yacoby, High-fidelity entangling gate for double-quantum-dot spin qubits, *npj Quantum Inf.* **3**, 3 (2017).
- [7] D. M. Zajac, T. M. Hazard, X. Mi, E. Nielsen, and J. R. Petta, Scalable Gate Architecture for a One-Dimensional Array of Semiconductor Spin Qubits, *Phys. Rev. Appl.* **6**, 054013 (2016).
- [8] L. M. K. Vandersypen, H. Bluhm, J. S. Clarke, A. S. Dzurak, R. Ishihara, A. Morello, D. J. Reilly, L. R. Schreiber, and M. Veldhorst, Interfacing spin qubits in quantum dots and donors—hot, dense, and coherent, *npj Quantum Inf.* **3**, 34 (2017).
- [9] R. Li, L. Petit, D. P. Franke, J. P. Dehollain, J. Helsen, M. Steudtner, N. K. Thomas, Z. R. Yoscovits, K. J. Singh, S. Wehner, *et al.*, A crossbar network for silicon quantum dot qubits, *Sci. Adv.* **4**, eaar3960 (2018).
- [10] A. M. J. Zwerver, T. Krähenmann, T. F. Watson, L. Lampert, H. C. George, R. Pillarisetty, S. A. Bojarski, P. Amin, S. V. Amitonov, J. M. Boter, *et al.*, Qubits made by advanced semiconductor manufacturing, *Nat. Electron.* **5**, 184 (2022).
- [11] X. Xue, M. Russ, N. Samkharadze, B. Undseth, A. Sammak, G. Scappucci, and L. M. K. Vandersypen, Quantum logic with spin qubits crossing the surface code threshold, *Nature* **601**, 343 (2022).
- [12] A. Noiri, K. Takeda, T. Nakajima, T. Kobayashi, A. Sammak, G. Scappucci, and S. Tarucha, Fast universal quantum gate above the fault-tolerance threshold in silicon, *Nature* **601**, 338 (2022).
- [13] M. T. Mądzik, S. Asaad, A. Youssef, B. Joecker, K. M. Rudinger, E. Nielsen, K. C. Young, T. J. Proctor, A. D. Baczewski, A. Laucht, *et al.*, Precision tomography of a three-qubit donor quantum processor in silicon, *Nature* **601**, 348 (2022).
- [14] A. R. Mills, C. R. Guinn, M. J. Gullans, A. J. Sigillito, M. M. Feldman, E. Nielsen, and J. R. Petta, Two-qubit silicon quantum processor with operation fidelity exceeding 99%, *Sci. Adv.* **8**, eabn5130 (2022).
- [15] R. Raussendorf and J. Harrington, Fault-Tolerant Quantum Computation with High Threshold in Two Dimensions, *Phys. Rev. Lett.* **98**, 190504 (2007).
- [16] A. G. Fowler, M. Mariantoni, J. M. Martinis, and A. N. Cleland, Surface codes: Towards practical large-scale quantum computation, *Phys. Rev. A* **86**, 032324 (2012).
- [17] T. Hensgens, T. Fujita, L. Janssen, X. Li, C. J. Van Diepen, C. Reichl, W. Wegscheider, S. Das Sarma, and L. M. K. Vandersypen, Quantum simulation of a Fermi-Hubbard model using a semiconductor quantum dot array, *Nature* **548**, 70 (2017).
- [18] J. P. Dehollain, U. Mukhopadhyay, V. P. Michal, Y. Wang, B. Wunsch, C. Reichl, W. Wegscheider, M. S. Rudner, E. Demler, and L. M. K. Vandersypen, Nagaoka ferromagnetism observed in a quantum dot plaquette, *Nature* **579**, 528 (2020).
- [19] M. Kiczynski, S. K. Gorman, H. Geng, M. B. Donnelly, Y. Chung, Y. He, J. G. Keizer, and M. Simmons, Engineering topological states in atom-based semiconductor quantum dots, *Nature* **606**, 694 (2022).

- [20] J. Preskill, Quantum computing and the entanglement frontier, arXiv preprint arXiv:1203.5813 (2012).
- [21] A. Laucht, R. Kalra, J. T. Muhonen, J. P. Dehollain, F. A. Mohiyaddin, F. Hudson, J. C. McCallum, D. N. Jamieson, A. S. Dzurak, and A. Morello, High-fidelity adiabatic inversion of a  $^{31}\text{P}$  electron spin qubit in natural silicon, *Appl. Phys. Lett.* **104**, 092115 (2014).
- [22] T. Albash and D. A. Lidar, Adiabatic quantum computation, *Rev. Mod. Phys.* **90**, 015002 (2018).
- [23] X. Chen, I. Lizuain, A. Ruschhaupt, D. Guéry-Odelin, and J. G. Muga, Shortcut to Adiabatic Passage in Two- and Three-Level Atoms, *Phys. Rev. Lett.* **105**, 123003 (2010).
- [24] D. Guéry-Odelin, A. Ruschhaupt, A. Kiely, E. Torrontegui, S. Martínez-Garaot, and J. G. Muga, Shortcuts to adiabaticity: Concepts, methods, and applications, *Rev. Mod. Phys.* **91**, 045001 (2019).
- [25] Y. Ban, X. Chen, E. Y. Sherman, and J. G. Muga, Fast and Robust Spin Manipulation in a Quantum Dot by Electric Fields, *Phys. Rev. Lett.* **109**, 206602 (2012).
- [26] A. Baksic, H. Ribeiro, and A. A. Clerk, Speeding up Adiabatic Quantum State Transfer by Using Dressed States, *Phys. Rev. Lett.* **116**, 230503 (2016).
- [27] M. V. Berry, Transitionless quantum driving, *J. Phys. A: Math. Theor.* **42**, 365303 (2009).
- [28] T. Wang, Z. Zhang, L. Xiang, Z. Jia, P. Duan, W. Cai, Z. Gong, Z. Zong, M. Wu, J. Wu, *et al.*, The experimental realization of high-fidelity ‘shortcut-to-adiabaticity’ quantum gates in a superconducting Xmon qubit, *New J. of Phys.* **20**, 065003 (2018).
- [29] W. Zheng, Y. Zhang, Y. Dong, J. Xu, Z. Wang, X. Wang, Y. Li, D. Lan, J. Zhao, S. Li, *et al.*, Optimal control of stimulated Raman adiabatic passage in a superconducting qubit, *npj Quantum Inf.* **8**, 9 (2022).
- [30] B. B. Zhou, A. Baksic, H. Ribeiro, C. G. Yale, F. J. Heremans, P. C. Jerger, A. Auer, G. Burkard, A. A. Clerk, and D. D. Awschalom, Accelerated quantum control using superadiabatic dynamics in a solid-state lambda system, *Nat. Phys.* **13**, 330 (2017).
- [31] J. Zhang, J. H. Shim, I. Niemeyer, T. Taniguchi, T. Teraji, H. Abe, S. Onoda, T. Yamamoto, T. Ohshima, J. Isoya, and D. Suter, Experimental Implementation of Assisted Quantum Adiabatic Passage in a Single Spin, *Phys. Rev. Lett.* **110**, 240501 (2013).
- [32] M. G. Bason, M. Viteau, N. Malossi, P. Huillery, E. Arimondo, D. Ciampini, R. Fazio, V. Giovannetti, R. Mannella, and O. Morsch, High-fidelity quantum driving, *Nat. Phys.* **8**, 147 (2012).
- [33] Y.-X. Du, Z.-T. Liang, Y.-C. Li, X.-X. Yue, Q.-X. Lv, W. Huang, X. Chen, H. Yan, and S.-L. Zhu, Experimental realization of stimulated Raman shortcut-to-adiabatic passage with cold atoms, *Nat. Commun.* **7**, 12479 (2016).
- [34] E. Boyers, P. J. D. Crowley, A. Chandran, and A. O. Sushkov, Exploring 2D Synthetic Quantum Hall Physics with a Quasiperiodically Driven Qubit, *Phys. Rev. Lett.* **125**, 160505 (2020).
- [35] S. G. J. Philips, M. T. Mađzik, S. V. Amitonov, S. L. de Snoo, M. Russ, N. Kalhor, C. Volk, W. I. L. Lawrie, D. Brousse, L. Trypuzen, *et al.*, Universal control of a six-qubit quantum processor in silicon, *Nature* **609**, 919 (2022).
- [36] K. C. Nowack, F. H. L. Koppens, Y. V. Nazarov, and L. M. K. Vandersypen, Coherent Control of a Single Electron Spin with Electric Fields, *Science* **318**, 1430 (2007).
- [37] X. Croot, X. Mi, S. Putz, M. Benito, F. Borjans, G. Burkard, and J. R. Petta, Flopping-mode electric dipole spin resonance, *Phys. Rev. Res.* **2**, 012006(R) (2020).
- [38] R. Hanson, B. Witkamp, L. M. K. Vandersypen, L. H. Willems van Beveren, J. M. Elzerman, and L. P. Kouwenhoven, Zeeman Energy and Spin Relaxation in a One-Electron Quantum Dot, *Phys. Rev. Lett.* **91**, 196802 (2003).
- [39] J. M. Elzerman, R. Hanson, L. H. Willems van Beveren, B. Witkamp, L. M. K. Vandersypen, and L. P. Kouwenhoven, Single-shot read-out of an individual electron spin in a quantum dot, *Nature* **430**, 431 (2004).
- [40] D. Keith, S. K. Gorman, L. Kranz, Y. He, J. G. Keizer, M. A. Broome, and M. Y. Simmons, Benchmarking high fidelity single-shot readout of semiconductor qubits, *New J. of Phys.* **21**, 063011 (2019).
- [41] C. Barthel, M. Kjaergaard, J. Medford, M. Stopa, C. M. Marcus, M. P. Hanson, and A. C. Gossard, Fast sensing of double-dot charge arrangement and spin state with a radio-frequency sensor quantum dot, *Phys. Rev. B* **81**, 161308(R) (2010).
- [42] D. J. Reilly, C. M. Marcus, M. P. Hanson, and A. C. Gossard, Fast single-charge sensing with a rf quantum point contact, *Appl. Phys. Lett.* **91**, 162101 (2007).
- [43] M. Shafiei, K. C. Nowack, C. Reichl, W. Wegscheider, and L. M. K. Vandersypen, Resolving Spin-Orbit- and Hyperfine-Mediated Electric Dipole Spin Resonance in a Quantum Dot, *Phys. Rev. Lett.* **110**, 107601 (2013).
- [44] C. Zener, Non-adiabatic crossing of energy levels, *Proc. R. Soc. A* **137**, 696 (1932).
- [45] C. Wittig, The Landau-Zener Formula, *J. Phys. Chem. B* **109**, 8428 (2005).
- [46] T. Nakajima, A. Noiri, K. Kawasaki, J. Yoneda, P. Stano, S. Amaha, T. Otsuka, K. Takeda, M. R. Delbecq, G. Allison, A. Ludwig, A. D. Wieck, D. Loss, and S. Tarucha, Coherence of a Driven Electron Spin Qubit Actively Decoupled from Quasistatic Noise, *Phys. Rev. X* **10**, 011060 (2020).
- [47] F. K. Malinowski, F. Martins, L. Cywiński, M. S. Rudner, P. D. Nissen, S. Fallahi, G. C. Gardner, M. J. Manfra, C. M. Marcus, and F. Kuemmeth, Spectrum of the Nuclear Environment for GaAs Spin Qubits, *Phys. Rev. Lett.* **118**, 177702 (2017).
- [48] E. J. Connors, J. Nelson, L. F. Edge, and J. M. Nichol, Charge-noise spectroscopy of Si/SiGe quantum dots via dynamically-decoupled exchange oscillations, *Nat. Commun.* **13**, 940 (2022).